*axioms*

MDPI

*Article*

# Thermoelastic Modeling of Fiber-Reinforced Composites with Gravity and Variable Reference Temperature: A Dual-Phase Green–Naghdi Theory Approach

**Samia M. Said [1,*], Emad K. Jaradat [2], Sayed M. Abo-Dahab [3] and Sarhan Y. Atwa [4]**

[1] Department of Mathematics, Faculty of Science, Zagazig University, Zagazig P.O. Box 44519, Egypt
[2] Department of Physics, Faculty of Science, Imam Mohammad Ibn Saud Islamic University (IMSIU), Riyadh 11623, Saudi Arabia; ekyjaradat@imamu.edu.sa
[3] Mathematics Department, Faculty of Science, South Valley University, Qena P.O. Box 83523, Egypt; elsayed.khodeari@sci.svu.edu.eg
[4] Department of Physics and Engineering Mathematics, Higher Institute of Engineering El-Shorouk Academy, El-Shorouk P.O. Box 11837, Egypt; srhan_1@yahoo.com
* Correspondence: samia_said59@yahoo.com

**Abstract**

An investigation is presented into the coupled thermo-mechanical behavior of a fiber-reinforced composite solid, with specific consideration given to the influences of gravity and thermal preconditions under inclined loading. The theoretical foundation of this work is based on the generalized dual-phase Green–Naghdi theory for constitutive modeling. Normal mode analysis has been utilized in the fundamental equations of coupled thermoelasticity. Ultimately, the derived equations are expressed as a vector-matrix differential equation, which is subsequently solved using the eigenvalue method. The outcomes of this analysis are then interpreted through numerical simulations, the details of which are presented graphically and discussed comprehensively to draw pertinent conclusions. A detailed parametric study was conducted to elucidate the individual and synergistic effects of these parameters on the material's behavior. The findings confirm the model's efficacy in capturing complex thermo-mechanical couplings, providing a robust framework for the design and optimization of composite structures in different environments. Analysis of the results indicates that the gravity field, reference temperature, and inclined load all exert a notable influence on the physical field variables. Furthermore, the numerical calculations performed in MATLAB R2013a demonstrate close consistency with the theoretical solution, verifying the model's accuracy.

**Keywords:** thermoelastic fiber-reinforced composite; the dual-phase Green–Naghdi framework; reference temperature; an eigenvalue-based formulation

**MSC:** 74F05; 74E30; 74B05

Check for updates

Academic Editor: Shengda Zeng

Received: 8 March 2026
Revised: 5 April 2026
Accepted: 13 April 2026
Published: 14 May 2026

**Copyright:** © 2026 by the authors. Licensee MDPI, Basel, Switzerland. This article is an open access article distributed under the terms and conditions of the Creative Commons Attribution (CC BY) license.

## 1. Introduction

The field of thermoelasticity has undergone significant theoretical evolution, driven by the development of increasingly sophisticated models to characterize the intricate coupling between thermal and mechanical fields in advanced engineering materials. Foundational work in this domain was established by Biot [1] through the pioneering principles of thermoelasticity and irreversible thermodynamics. In parallel, seminal research on fiber-reinforced composites by Belfield et al. [2] provided critical frameworks for stress

analysis and mechanical behavior in these complex, anisotropic media, forming a cornerstone for subsequent analytical studies. Chattopadhyay and Choudhury [3] examined the spread of magnetoelastic shear waves in an infinitely self-reinforced medium. Sengupta and Nath [4] conducted a study on surface waves within anisotropic, fiber-reinforced, solid elastic media. The study by Singh [5] examined the spread of Rayleigh waves in a thermally insulated, fiber-reinforced thermoelastic medium half-space. An advanced application within this context is demonstrated by the work of Sarkar and Atwa [6] who employed the Green–Naghdi hypothesis to investigate the consequence of a crack on the two-temperature thermoelastic behavior of a fibre-reinforced composite. Numerous studies on fiber-reinforced thermoelastic media can be found in Refs. [7–11].

A cornerstone of this evolution is the Green–Naghdi theory [12], which introduced a rigorous framework for thermoelasticity without energy dissipation, thereby ensuring finite wave speeds and enabling more realistic modeling of transient thermal-mechanical interactions. This foundational work has catalyzed the development of numerous generalized models tailored to specific physical complexities. The spreading of time-harmonic plane thermoelastic waves with a specified frequency in a boundless rotating material is analyzed using the Green–Naghdi model of linear thermoelasticity without energy dissipation, as studied by Roychoudhuri and Bandyopadhyay [13]. Magneto-thermoelastic interactions in an initially stressed isotropic elastic half-space with dual temperature effects were analyzed using mathematical approaches within the framework of the Green–Naghdi hypothesis, as discussed by Atwa [14]. Abo-Dahab et al. [15] discussed a problem of magneto-thermoelastic half-space subjected to time-dependent heat source via Green-Naghdi's second model (GN-II) of thermoelasticity. Zenkour [16] introduced innovative multi-single/dual-phase-lag frameworks to explore the thermoelastic diffusion behavior of a solid. The effect of gravitational body forces on the thermoelastic response, a factor of paramount importance in structural and geotechnical applications, was rigorously analyzed within the Green–Naghdi framework by Othman and Said [17]. Recently, Tzou [18] proposed the dual-phase-lag (DPL) model, which describes the interactions between phonons and electrons on the microscopic level as retarding sources causing a delayed response on the macroscopic scale. Green–Naghdi (GN) Type III and dual-phase-lag (DPL) models are essential for modeling accurate thermoelastic behavior in advanced materials under extreme, fast-acting, or ultra-short pulse conditions. These theories improve upon classical Fourier heat conduction by providing finite heat wave speeds, eliminating nonphysical instantaneous heat propagation. They are critical in high-tech fields like nano-material manufacturing, laser technology, and aerospace. Numerous studies utilizing the Green–Naghdi theory to analyze various thermoelastic materials are available in the literature, as referenced in [19–21].

Recent studies have underscored the critical importance of accounting for the temperature-dependent nature of material properties in accurate modeling. Subsequent research has significantly extended this framework to incorporate a wider array of physical phenomena. The thermal stress on a material with temperature-dependent properties has been thoroughly investigated by Noda [22]. Key material properties, including the modulus of elasticity and thermal conductivity, are observed to change with temperature. The critical influence of a material's elastic properties varying with a reference temperature was formally integrated into generalized thermoelasticity by Ezzat et al. [23], addressing a key aspect of material behavior in non-isothermal environments. The study by Othman et al. [24] examined a thermoelastic solid with temperature-dependent properties, considering various hypotheses under the influence of a gravitational field. Numerous studies have explored various thermoelastic materials with temperature-dependent properties, as documented in references [25–33].

We introduced a comprehensive model for the thermomechanical behavior of fiber-reinforced composites that simultaneously incorporates the influences of gravitational body forces and variable temperature-dependent material properties within a dual-phase Green–Naghdi framework. This study's purpose is to develop a theoretical framework that integrates these critical factors, seeking to provide a broader analytical framework for understanding the behavior of such composites under a more comprehensive set of physical conditions. The continuous advancement of thermoelasticity theory is marked by the development of refined frameworks capable of analyzing material performance under combined thermal and mechanical loads. Analysis of the results indicates that the gravity field, reference temperature, and inclined load all exert a notable influence on the physical field variables.

## 2. The Description of the System

A problem of a fiber-reinforced thermoelastic medium under varying reference temperature in $xz$ plane under the impact of gravitational and inclined loading as in Figure 1. The field equations and constitutive relations are given by Belfield et al. [2] based on the principles of generalized thermoelasticity. The constitutive relations take the following form:

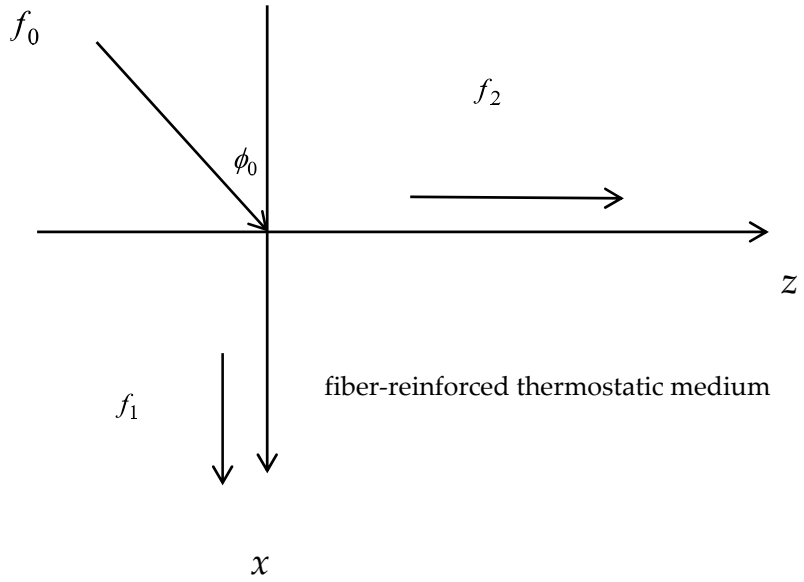



**Figure 1.** The diagram of the problem.

I. **The material constitutive laws**

$$\sigma_{ij} = \lambda\, e_{kk}\, \delta_{ij} + 2\mu_T\, e_{ij} + \alpha(b_k\, b_m\, e_{km}\, \delta_{ij} + b_i\, b_j\, e_{kk}) + 2(\mu_L - \mu_T)(b_i\, b_k\, e_{kj} + b_j\, b_k\, e_{ki}) + \beta\, b_k\, b_m\, e_{km}\, b_i\, b_j - \gamma\, \theta\, \delta_{ij}\,. \tag{1}$$

II. **The equations of dynamic equilibrium**

$$\rho\, \ddot{u}_i = \sigma_{ji,\,j} + F_i,\, F_1 = \rho\, g \frac{\partial\, u_3}{\partial x},\, F_2 = 0,\, F_3 = -\rho\, g \frac{\partial\, u_1}{\partial x}. \tag{2}$$

III. **The governing equation for heat transfer**

According to the dual-phase-lag (DPL) extension of the Green–Naghdi hypothesis, the governing heat conduction equation takes the following refined form, which is employed (see also Zenkour [16]):

$$K\left(\frac{\partial}{\partial t}+\frac{E\,K^{*}}{K}\left(1+\sum_{\ell=1}^{N}\frac{\tau_{\theta}^{\ell}}{\ell!}\frac{\partial^{\ell}}{\partial t^{\ell}}\right)\right)\nabla^{2}\theta=\left(1+\sum_{\Lambda=1}^{M}\frac{\tau_{q}^{\Lambda}}{\Lambda!}\frac{\partial^{\Lambda}}{\partial t^{\Lambda}}\right)\frac{\partial^{2}}{\partial t^{2}}(\rho\,C_{E}\theta+\gamma\,T_{0}\,e). \tag{3}$$

Some special cases may be obtained from Equation (3), such as:

(a) Dual-phase-lag G-N type III model: $M=N\geq 1$.
(b) Simple-phase-lag G-N type III model: $\tau_{\theta}=0,\quad M=1$.
(c) Simple-phase-lag G-N type II model: $\tau_{\theta}=K^{*}=0,\quad M=1$.
(d) G–N type III model: $\tau_{\theta}=\tau_{q}=0$.
(e) G–N type II model: $K^{*}=\tau_{\theta}=\tau_{q}=0$.

We acquire that as Ezzat et al. [23]:

$$\mu=\mu_{0}\,f(T),\,\mu_{L}=\mu_{L_{0}}\,f(T),\,\mu_{T}=\mu_{T_{0}}\,f(T),\,\lambda=\lambda_{0}\;f(T),\,\beta=\beta_{0}\;f(T),\,\alpha=\alpha_{0}\,f(T), \tag{4}$$

where $f(T)=(1-\theta_{0}T_{0})$ and $\theta_{0}$ is an empirical constant of the solid. In this case, the elastic modulus is temperature-insensitive if $\theta_{0}=0$.

This relationship is obtained by substituting Equation (1) into Equation (2), resulting in:

$$\rho\,\frac{\partial^{2}u_{1}}{\partial\,t^{2}}=A_{1}\,\frac{\partial^{2}u_{1}}{\partial\,x^{2}}+A_{4}\frac{\partial^{2}u_{3}}{\partial\,x\,\partial\,z}+\mu_{L}\;\frac{\partial^{2}u_{1}}{\partial\,z^{2}}-\gamma\,\frac{\partial\theta}{\partial\,x}\;+\rho g\frac{\partial\,u_{3}}{\partial\,x}, \tag{5}$$

$$\rho\;\;\frac{\partial^{2}u_{3}}{\partial\,t^{2}}=\mu_{L}\;\;\frac{\partial^{2}u_{3}}{\partial\,x^{2}}+A_{4}\frac{\partial^{2}u_{1}}{\partial\,x\,\partial z}+A_{3}\,\frac{\partial^{2}u_{3}}{\partial\,z^{2}}-\gamma\,\frac{\partial\theta}{\partial\,z}\;-\rho g\frac{\partial\,u_{1}}{\partial\,x}, \tag{6}$$

where,

$A_{1}=\lambda+2\alpha+4\mu_{L}-2\mu_{T}+\beta$, $A_{2}=\lambda+\alpha$, $A_{3}=\lambda+2\mu_{T}$, $A_{4}=\lambda+\alpha+\mu_{L}$.

The analysis is simplified by introducing the dimensionless quantities below:

$$(x',\,z',\,u'_{1},\,u'_{3})=c_{0}\eta\,(x,\,z,\,u_{1},\,u_{3}),\,(t',\,\tau'_{q},\,\tau'_{\theta})=c_{0}^{2}\eta\,(t,\,\tau_{q},\,\tau_{\theta}),\,\theta'=\frac{\gamma\theta}{A_{3}},\,\sigma'_{ij}=\frac{\sigma_{ij}}{\mu_{T}},\,g'=\frac{g}{\eta\,c_{0}^{3}}, \tag{7}$$

where,

$\eta=\frac{\rho\,C_{E}}{K^{*}}$, $c_{0}^{2}=\frac{\lambda_{0}+2\mu_{T_{0}}}{\rho}$.

With the aid of Equation (7), Equations (3), (5) and (6) are reformulated as follows:

$$\frac{\partial^{2}u_{1}}{\partial\,t^{2}}=A_{5}\frac{\partial^{2}u_{1}}{\partial\,x^{2}}+A_{6}\frac{\partial^{2}u_{3}}{\partial\,x\,\partial z}+A_{7}\frac{\partial^{2}u_{1}}{\partial\,z^{2}}-\frac{\partial\,\theta}{\partial\,x}+g\frac{\partial u_{3}}{\partial\,x}, \tag{8}$$

$$\frac{\partial^{2}u_{3}}{\partial\,t^{2}}=A_{7}\frac{\partial^{2}u_{3}}{\partial\,x^{2}}+A_{6}\frac{\partial^{2}u_{1}}{\partial x\,\partial\,z}+A_{8}\frac{\partial^{2}u_{3}}{\partial\,z^{2}}-\frac{\partial\,\theta}{\partial\,z}-g\frac{\partial\,u_{1}}{\partial\,x}, \tag{9}$$

$$\left(A_{9}\frac{\partial}{\partial t}+A_{0}\left(1+\sum_{\ell=1}^{N}\frac{\tau_{\theta}^{\ell}}{\ell!}\frac{\partial^{\ell}}{\partial t^{\ell}}\right)\right)\nabla^{2}\theta=\left(1+\sum_{\Lambda=1}^{M}\frac{\tau_{q}^{\Lambda}}{\Lambda!}\frac{\partial^{\Lambda}}{\partial t^{\Lambda}}\right)\frac{\partial^{2}}{\partial t^{2}}(A_{10}\theta+A_{11}\,e), \tag{10}$$

where,

$A_{5}=\frac{A_{1}}{\rho\,c_{0}^{2}}$, $A_{6}=\frac{A_{4}}{\rho\,c_{0}^{2}}$, $A_{7}=\frac{\mu_{L}}{\rho\,c_{0}^{2}}$, $A_{8}=\frac{A_{3}}{\rho\,c_{0}^{2}}$, $A_{9}=\frac{K\,c_{0}^{4}\,\eta^{3}\,(\lambda+2\mu_{T})}{\gamma}$, $A_{10}=\frac{\rho\,C_{E}\,\eta^{2}\,c_{0}^{4}\,(\lambda+2\mu_{T})}{\gamma}$, $A_{0}=\frac{EK^{*}\eta^{2}\,c_{0}^{2}\,(\lambda+2\mu_{T})}{\gamma}$, $A_{11}=\gamma\,T_{0}c_{0}^{4}\,\eta^{2}$.

## 3. Problem Solution Technique

The physical fields are expressed using normal mode analysis.

$$\left[u_1, u_3, \theta, \sigma_{ij}\right](x,z,t) = \left[\widetilde{u}_1, \widetilde{u}_3, \widetilde{\theta}, \widetilde{\sigma}_{ij}\right](z)\ \exp(\mathrm{i}\varsigma\, x - mt). \tag{11}$$

Introducing Equation (11) in (8)–(10), we get

$$\mathrm{D}^2\widetilde{u}_1 = M_{11}\widetilde{u}_1 + M_{12}\widetilde{u}_3 + M_{13}\widetilde{\theta} + M_{15}\mathrm{D}\,\widetilde{u}_3, \tag{12}$$

$$\mathrm{D}^2\widetilde{u}_3 = M_{21}\widetilde{u}_1 + M_{22}\widetilde{u}_3 + M_{24}\mathrm{D}\widetilde{u}_1 + M_{26}\mathrm{D}\,\widetilde{\theta}, \tag{13}$$

$$\mathrm{D}^2\widetilde{\theta} = M_{31}\widetilde{u}_1 + M_{33}\,\widetilde{\theta} + M_{35}\mathrm{D}\widetilde{u}_3, \tag{14}$$

where,

$M_{11} = \frac{A_5\,\varsigma^2+m^2}{A_7}$, $M_{12} = \frac{-\mathrm{i}g\varsigma}{A_7}$, $M_{13} = \frac{\mathrm{i}\varsigma}{A_7}$, $M_{15} = \frac{-\mathrm{i}\varsigma\,A_6}{A_7}$, $M_{21} = \frac{\mathrm{i}g\varsigma}{A_8}$, $M_{22} = \frac{A_7\varsigma^2+m^2}{A_8}$, $M_{24} = -\frac{\mathrm{i}A_6\,\varsigma}{A_8}$, $M_{26} = \frac{1}{A_8}$, $M_{31} = \frac{\mathrm{i}A_{15}\,\varsigma}{A_{13}}$, $M_{33} = \frac{A_{14}+A_{13}\varsigma^2}{A_{13}}$, $M_{35} = \frac{A_{15}}{A_{13}}$, $A_{13} = -A_9 m + A_0(1+\sum_{n=1}^{N}\frac{\tau_\theta^\ell}{\ell!}(-m)^\ell)$, $A_{14} = A_{10}m^2(1+\sum_{\Lambda=1}^{M}\frac{\tau_q^\Lambda}{\Lambda!}(-m)^\Lambda)$, $A_{15} = A_{11}m^2(1+\sum_{\Lambda=1}^{M}\frac{\tau_q^\Lambda}{\Lambda!}(-m)^\Lambda)$, $\mathrm{D} = \frac{\mathrm{d}}{\mathrm{d}\,z}$.

Following Das and Lahiri [34], Equations (12)–(14) can be combined and represented in a compact vector-matrix differential form.

$$\mathrm{D}V(z) = A(\varsigma, m)V(z), \tag{15}$$

where,

$V(z) = [\widetilde{u}_1, \widetilde{u}_3, \widetilde{\theta}, D\widetilde{u}_1, D\widetilde{u}_3, D\widetilde{\theta}]^{\mathrm{T}}$

$$A = \begin{bmatrix} 0 & 0 & 0 & 1 & 0 & 0 \\ 0 & 0 & 0 & 0 & 1 & 0 \\ 0 & 0 & 0 & 0 & 0 & 1 \\ M_{11} & M_{12} & M_{13} & 0 & M_{15} & 0 \\ M_{21} & M_{22} & 0 & M_{24} & 0 & M_{26} \\ M_{31} & 0 & M_{33} & 0 & M_{35} & 0 \end{bmatrix} \tag{16}$$

Introducing the eigenvalue formulation as Das and Lahiri [34], the characteristic equation associated with the matrix formulation in Equation (16) is derived as follows:

$$\Gamma^6 - n_1\,\Gamma^4 + n_2\,\Gamma^2 - n_3\ = 0, \tag{17}$$

where

$$\begin{aligned} n_1 &= M_{35}\,M_{26} + M_{15}\,M_{24} + M_{33} + M_{22} + M_{11}, \\ n_2 &= -M_{13}M_{35}\,M_{24} + M_{33}M_{15}\,M_{24} + M_{22}M_{33} + M_{26}M_{35}M_{11} - M_{15}M_{31}M_{26} + \\ &\quad M_{11}M_{33} - M_{13}M_{31} + M_{11}M_{22} - M_{21}M_{12}, \\ n_3 &= M_{11}M_{22}\,M_{33} - M_{21}\,M_{12}M_{33} - M_{13}\,M_{31}M_{22}, \end{aligned}$$

Let $\Gamma_1^2$, $\Gamma_2^2$, $\Gamma_3^2$ be the roots of Equation (17) with real positive parts. Then all six roots of the above characteristic equation, which are also the eigenvalues of the matrix $A$, will be

of form $\Gamma = \pm\,\Gamma_1,\ \pm\,\Gamma_2,\ \pm\,\Gamma_3$. For the eigenvalue $\Gamma$ of the matrix $A$, the six eigenvector $\chi = [x_1, x_2, x_3, x_4, x_5, x_6]^T$.

$$x_1 = -\Gamma_j\, M_{26}(M_{12} + \Gamma_j\, M_{15}) - (\Gamma_j^2 - M_{22})M_{13},$$

$$x_2 = -\Gamma_j\, M_{26}(\Gamma_j^2 - M_{11}) - (M_{21} + \Gamma_j M_{24})M_{13},$$

$$x_3 = (\Gamma_j^2 - M_{11})(\Gamma_j^2 - M_{22}) - (M_{21} + \Gamma_j\, M_{24})(\, M_{12} + \Gamma_j\, M_{15}),$$

$$x_4 = \Gamma\, x_1,\ x_5 = \Gamma\, x_2,\quad x_6 = \Gamma\, x_3.$$

To calculate the eigenvector $\chi_j,\ (j = 1,\ 2,\ 3)$ corresponding to the eigenvalue $\pm\Gamma_j,\ (j = 1,\ 2,\ 3)$, we use the following notations:

$$\chi_1 = [\chi]_{\Gamma=\Gamma_1} \quad \chi_2 = [\chi]_{\Gamma=-\Gamma_1} \quad \chi_3 = [\chi]_{\Gamma=\Gamma_2} \quad \chi_4 = [\chi]_{\Gamma=-\Gamma_2} \quad \chi_5 = [\chi]_{\Gamma=\Gamma_3} \quad \chi_6 = [\chi]_{\Gamma=-\Gamma_3}.$$

The bounded solution to Equation (15) satisfies the following condition: $z \to \infty$, which yields

$$\widetilde{u}_1(z) = \sum_{j=1}^{3} R_j\, \Pi_{1j}\ \exp(-\Gamma_j z), \tag{18}$$

$$\widetilde{u}_3(z) = \sum_{j=1}^{3} R_j\, \Pi_{2j}\ \exp(-\Gamma_j\, z), \tag{19}$$

$$\widetilde{\theta}(z) = \sum_{j=1}^{3} R_j\, \Pi_{3j}\ \exp(-\Gamma_j\, z), \tag{20}$$

where,

$\Pi_{1j} = [x_1]_{\Gamma=-\Gamma_j}, \Pi_{2j} = [x_2]_{\Gamma=-\Gamma_j}, \Pi_{3j} = [x_3]_{\Gamma=-\Gamma_j}$.

Using Equations (18)–(20), we get

$$\widetilde{\sigma}_{zz}(z) = \sum_{j=1}^{3} R_j\, \Pi_{4j}\ \exp(-\Gamma_j\, z), \tag{21}$$

$$\widetilde{\sigma}_{xz}(z) = \sum_{j=1}^{3} R_j\, \Pi_{5j}\ \exp(-\Gamma_j\, z), \tag{22}$$

where,

$\Pi_{4j} = \frac{1}{\mu_T}\left(\mathrm{i}\varsigma\, A_2\Pi_{1j} - A_3\Gamma_j\Pi_{2j} - (\lambda + 2\mu_T)\Pi_{3j}\right), \Pi_{5j} = \frac{\mu_L}{\mu_T}\left(\mathrm{i}\varsigma\, \Pi_{2j} - \Gamma_j\Pi_{1j}\right)$.

## 4. Application

For the purpose of parameter determination, $R_j\ (j = 1,\ 2,\ 3)$ with the boundary conditions used in the analysis at $z = 0$ are applied:

(a) The surface of the solid remains at a constant temperature.

$$\theta = 0. \tag{23}$$

(b) Mechanical constraint enforcing a prescribed load on the external boundary of the solid as Lata and Kaur [35]

$$\sigma_{zz} = -f_0\ \cos(\phi_0), \qquad \sigma_{xz} = -f_0\ \sin(\phi_0), \tag{24}$$

where $f_0$ is a constant and $\phi_0$ is an inclined load angle.

Substituting the defined variables into the boundary conditions (23) and (24) gives the parameter equations:

$$\sum_{n=1}^{3} \Pi_{3n} R_n = 0, \sum_{n=1}^{3} \Pi_{4n} R_n = -f_0 \cos(\phi_0), \sum_{n=1}^{3} \Pi_{5n} R_n = -f_0 \sin(\phi_0). \tag{25}$$

The solution is obtained by applying the matrix inverse method, resulting in:

$$\begin{pmatrix} R_1 \\ R_2 \\ R_3 \end{pmatrix} = \begin{pmatrix} \Pi_{31} & \Pi_{32} & \Pi_{33} \\ \Pi_{41} & \Pi_{42} & \Pi_{43} \\ \Pi_{51} & \Pi_{52} & \Pi_{53} \end{pmatrix}^{-1} \begin{pmatrix} 0 \\ -f_0 \cos(\phi_0) \\ -f_0 \sin(\phi_0) \end{pmatrix}. \tag{26}$$

## 5. Numerical Computations and Analysis

To demonstrate the previous theoretical findings and investigate them using different versions of the dual-phase Green–Naghdi theory, we present numerical values for the physical constants, as in Othman et al. [8]. This analysis studies the effects of gravity, reference temperature, and inclined loading on a fiber-reinforced thermoelastic medium.

$$\lambda_0 = 7.76 \times 10^9 \,\mathrm{N{\cdot}m^{-2}}, \quad \mu_0 = 3.86 \times 10^9 \,\mathrm{N{\cdot}m^{-2}}, \quad \mu_{L0} = 7.86 \times 10^9 \,\mathrm{N{\cdot}m^{-2}}, \quad \mu_{T0} = 2.86 \times 10^9 \,\mathrm{N{\cdot}m^{-2}},$$

$$C_E = 383.1 \,\mathrm{J{\cdot}(kgk)^{-1}}, \quad K = 386 \,\mathrm{w{\cdot}(mk)^{-1}}, \quad m = m_0 + \mathrm{i}\,\xi, \quad m_0 = -1.5, \quad \xi = -0.5, \quad \tau_q = 0.9 \,\mathrm{s}, \quad \tau_\theta = 0.7 \,\mathrm{s},$$

$$\beta_0 = 2 \times 10^9 \,\mathrm{N{\cdot}m^{-2}}, \quad K^* = 386 \,\mathrm{w{\cdot}m^{-1}{\cdot}K^{-1}{\cdot}s^{-1}}, \quad \alpha_t = 1.78 \times 10^{-5} \,\mathrm{k^{-1}}, \quad \rho = 7400 \,\mathrm{kg{\cdot}m^{-3}}, \quad T_0 = 293 \,\mathrm{K},$$
$$f_0 = 2.5, \quad \varsigma = 0.3, \quad \alpha_0 = -1.78 \times 10^9 \,\mathrm{N{\cdot}m^{-2}}, \quad x = 0.5, \quad t = 1.01 \,\mathrm{s}.$$

Figures 2–5 analyze the differences in vertical displacement $u_3$, thermodynamic temperature $\theta$, as well as the stress components $\sigma_{zz}$ and $\sigma_{xz}$ under both gravitational and zero-gravity conditions. The behavior is discussed via three theoretical hypotheses: the dual-phase-lag Green–Naghdi type III (DPL G-N type III), the Green–Naghdi framework with single-phase-lag type III (SPL G-N type III), and classical Green–Naghdi (G–N) type III theories. Figure 2 introduces the spatial variation of vertical displacement $u_3$ in a continuous medium that is both thermoelastic and fiber-reinforced under the influence of various heat conduction frameworks in the presence and absence of a gravity field. In the presence of the gravity field ($g = 9.8 \,\mathrm{m \cdot s^{-2}}$), all models exhibit a significant downward and then upward displacement near the surface, with a smooth decline as the distance $z$ increases. Among them, the SPL G-N type III and classical G–N type III frameworks predict slightly higher displacement magnitudes compared to the DPL type III framework, indicating their sensitivity to phase-lag effects in heat transport. When a gravity field $g = 9.8$ is applied, a noticeable reduction in vertical displacement is observed across all frameworks. In the absence of the gravity field ($g = 0$), all models exhibit a decrease during the interval $0 \leq z \leq 10$. This suppression is due to the gravity field's damping impact, thereby inhibiting the motion of the medium. Figure 3 presents the distribution of thermal temperature across a range of heat conduction hypotheses in the presence and absence comparing scenarios with and without the effects of a gravity field. All models exhibit a significant upward reach maximum magnitude and then downward to reach a minimum magnitude near the surface, with a smooth decline toward zero as the distance $z$ increases. At larger values of $z$, all curves converge asymptotically to the same equilibrium state. Figure 4 displays the normal stress distribution $\sigma_{zz}$ under gravitational and non-gravitational conditions. In the presence of the gravity field, the curves exhibit a clear dip to a minimum magnitude, indicating the location of maximum compressive stress, followed by a gradual recovery toward zero as $z$ increases. When gravity is absent, the curves show an increasing trend within the interval $0 \leq z \leq 10$. Overall, the gravity induces magnification and localizes the mechanical stress effect, while the choice

of hypothesis significantly affects the predicted stress magnitude and profile. Figure 5 presents the variation in the shear stress component $\sigma_{xz}$ in relation to the spatial coordinate $z$, comparing the consequence in the absence of gravitational effects. The curves initially decrease sharply in the negative direction, reaching a peak before oscillating upward and gradually decaying, forming a wave pattern that starts downward. Conversely, in the presence of the gravity field, the curves start by increasing into the positive region before decreasing, maintaining the wave-like shape but with an initial upward trend. In both cases, the stress gradually decreases as increases $z$, indicating spatial attenuation of the stress response.

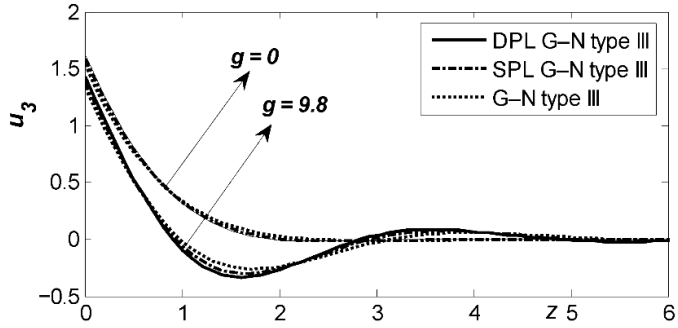



**Figure 2.** Vertical displacement dispersion $u_3$ in the absence and presence of the gravity field.

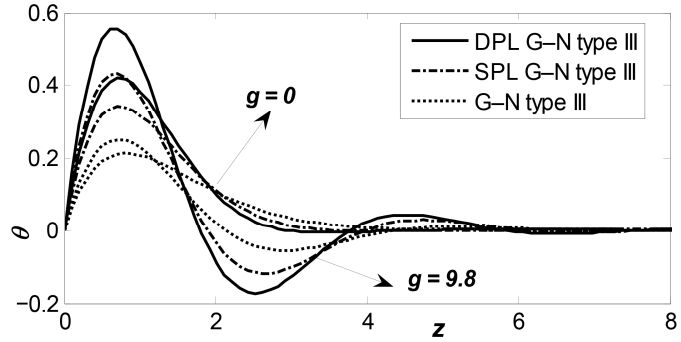



**Figure 3.** Thermodynamic temperature dispersion $\theta$ in the absence and presence of the gravity field.

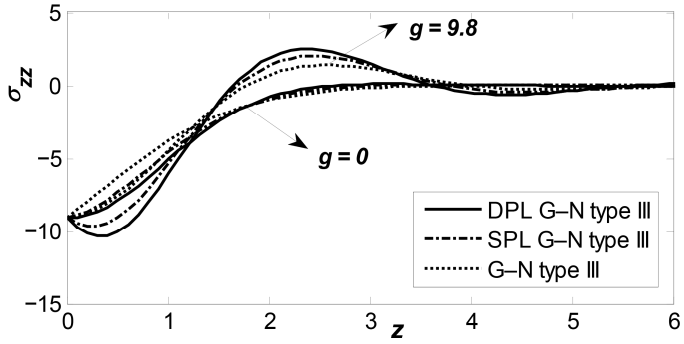



**Figure 4.** Organization of stress component $\sigma_{zz}$ in the absence and presence of the gravity field.

Figures 6–9 illustrate the behavior of $u_3$, $\theta$, $\sigma_{zz}$ and $\sigma_{xz}$ comparing two different values of reference temperature ($\theta_0 = 0.1\ \mathrm{K}^{-1}$, $0.9\ \mathrm{K}^{-1}$). Figure 6 describes the fluctuation of vertical displacement $u_3$ with the spatial coordinate $z$ for various frameworks. The numerical results show that all frameworks display a damp oscillatory trend as $z$ increases. Furthermore, the reference temperature amplifies the displacement amplitude. The classical G-N type III hypothesis is the most sensitive, followed by the SPL G-N type III framework, while the DPL G–N type III is the least affected. Figure 7 describes that the fluctuation

of thermodynamic temperature $\theta$ uses a zero starting point, then optimizes the boundary conditions. The curves start by increasing into the positive region before decreasing, maintaining the wave-like shape but with an initial upward trend. The DPL G–N type III hypothesis is the most sensitive, followed by the SPL G-N type III framework, while the classical G-N type III is the least affected. Figure 8 presents the fluctuation as well as the stress components; $\sigma_{zz}$ starts assuming a negative magnitude and adjusts for the boundary conditions. Overall, the reference temperature acts to amplify and localize the mechanical stress response, while the choice of hypothesis significantly affects the predicted stress magnitude and profile. Figure 9 presents the fluctuation for the stress component $\sigma_{xz}$, which begins at zero and modifies the boundary conditions. The values of $\sigma_{xz}$ decreases sharply to a minimum magnitude, then sharply to a maximum magnitude, and then gradually relaxes toward zero. It can be noted that the presence of the reference temperature displays a great impact on the magnitude of $\sigma_{xz}$. The classical G-N type III hypothesis is the most sensitive, followed by the SPL G-N type III framework, while the DPL G–N type III is the least affected.

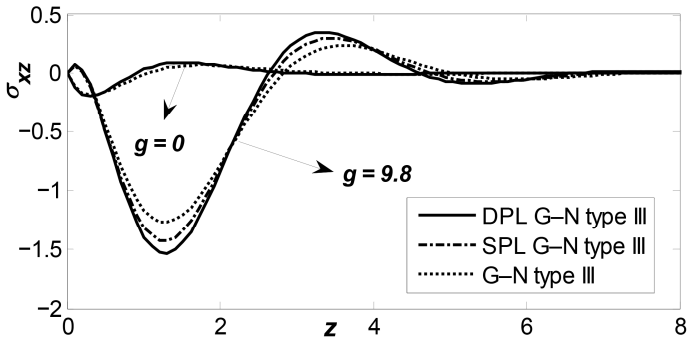



**Figure 5.** Organization of stress component $\sigma_{xz}$ in the absence and presence of the gravity field.

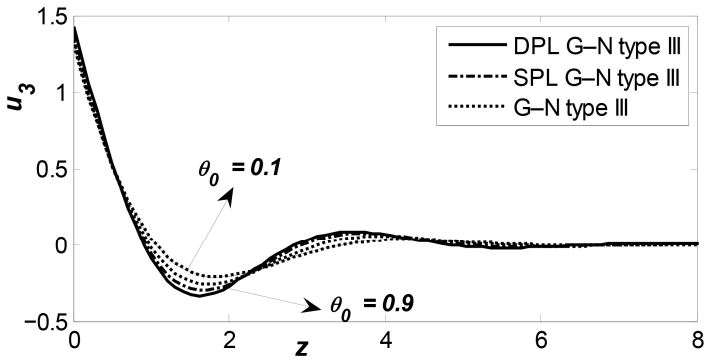



**Figure 6.** Vertical displacement dispersion $u_3$ in the absence and presence of reference temperature.

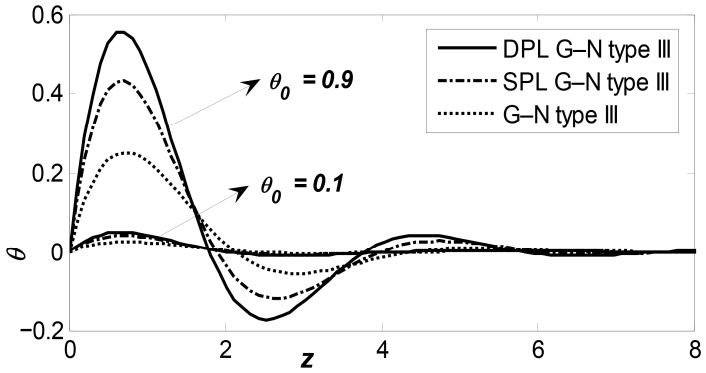



**Figure 7.** Thermodynamic temperature dispersion $\theta$ in the absence and presence of reference temperature.

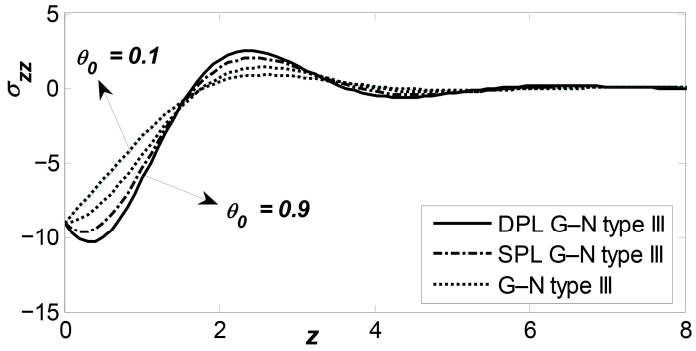



**Figure 8.** Organization of stress component $\sigma_{zz}$ in the absence and presence of reference temperature.

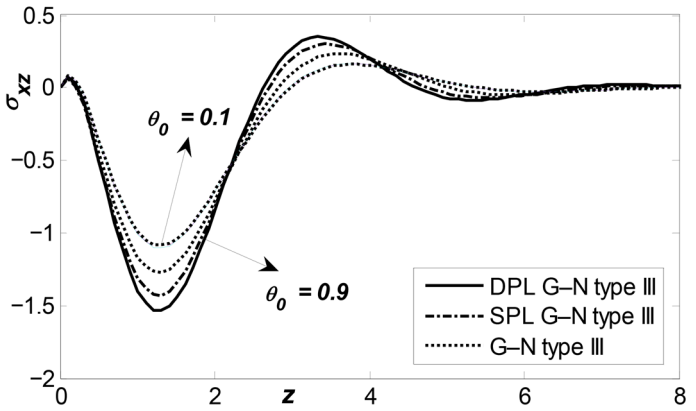



**Figure 9.** Organization of stress component $\sigma_{xz}$ in the absence and presence of reference temperature.

Figures 10–13 illustrate the comparative behavior of the vertical displacement component $u_3$, thermodynamic temperature $\theta$, and stress components $\sigma_{zz}$ and $\sigma_{xz}$ in the presence and absence of an inclined load. The behavior is discussed via three theoretical hypotheses: the dual-phase-lag Green–Naghdi type III (DPL G-N type III), Single-phase-lag Green–Naghdi type III (SPL G-N type III), and classical Green–Naghdi (G–N) type III frameworks. Figure 10 introduces the spatial variation of vertical displacement $u_3$ in a fiber-reinforced thermoelastic solid. This analysis uses multiple heat conduction frameworks and considers the effect of an inclined load. All models exhibit a significant downward and then upward displacement near the surface, with a smooth decline toward zero as the distance $z$ increases. There is suppression due to the inclined load damping impact, thereby inhibiting the motion of the medium. Figure 11 describes the fluctuation of thermodynamic temperature $\theta$ in the presence and absence of an inclined load versus the distance $z$. The curves start by increasing into the positive region before decreasing, maintaining the wave-like shape but with an initial upward trend. It is evident that the presence of an inclined load exerts a considerable influence on the thermodynamic temperature. Figure 12 presents the spatial distribution pattern for the normal stress component $\sigma_{xz}$ in the presence and absence of an inclined load. A distinct dip to a maximum magnitude is observed in the curves, followed by a subsequent decline, then by a gradual recovery towards zero as $z$ increases. Overall, the inclined load acts to magnify and localize the mechanical stress response, while the choice of hypothesis significantly affects the predicted stress magnitude and profile. Figure 13 depicts the variation in the shear stress component $\sigma_{xz}$ in relation to the spatial coordinate $z$ comparing the consequence of the inclined load. In the presence of the inclined load, the curves initially increase sharply in the positive direction, reaching a peak before oscillating downward and gradually decaying, forming a wave pattern that starts upward. Overall, the inclined load acts to amplify and localize the mechanical stress response, while the choice of hypothesis significantly affects the predicted stress

magnitude and profile. Figures 14 and 15 display 3D surface curves depicting physical quantities such as displacement and thermodynamic temperature. The plots, generated using the dual-phase-lag Green–Naghdi type III model, are critical for examining how gravity and an inclined load affect a fiber-reinforced thermoelastic solid with variable reference temperature, specifically focusing on their variation with vertical distance.

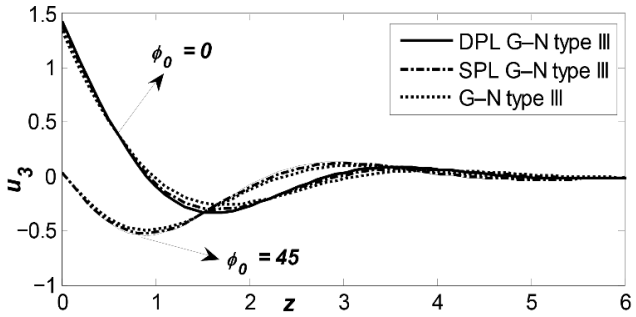



**Figure 10.** Vertical displacement dispersion $u_3$ in the absence and presence of an inclined load.

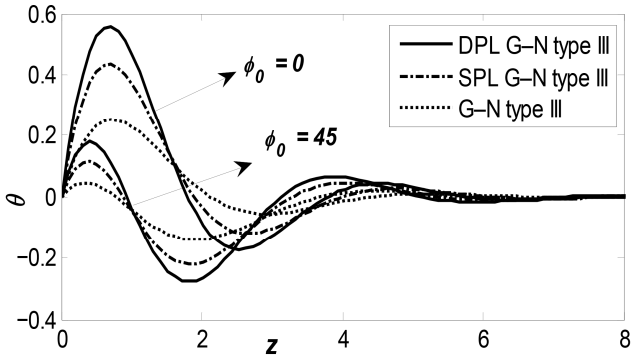



**Figure 11.** Thermodynamic temperature dispersion $\theta$ in the absence and presence of an inclined load.

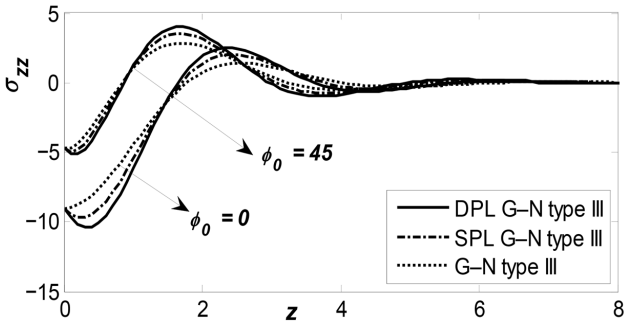



**Figure 12.** Organization of stress component $\sigma_{zz}$ in the absence and presence of an inclined load.

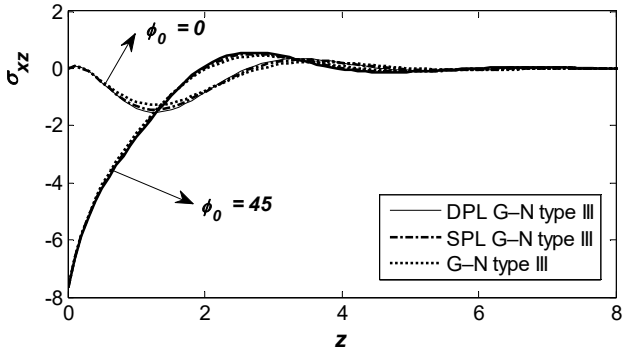



**Figure 13.** Organization of stress component $\sigma_{xz}$ in the absence and presence of an inclined load.

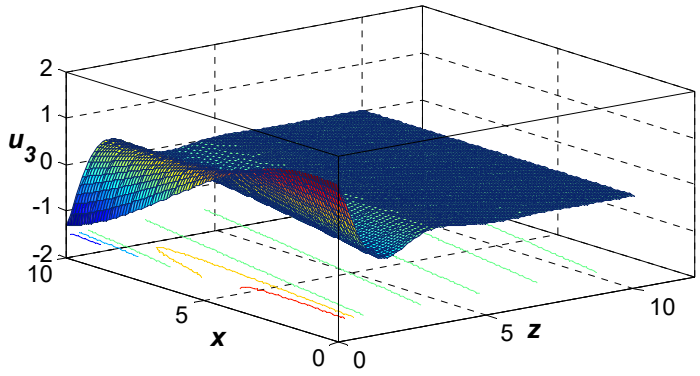



**Figure 14.** 3D Vertical displacement dispersion $u_3$ versus components of distance.

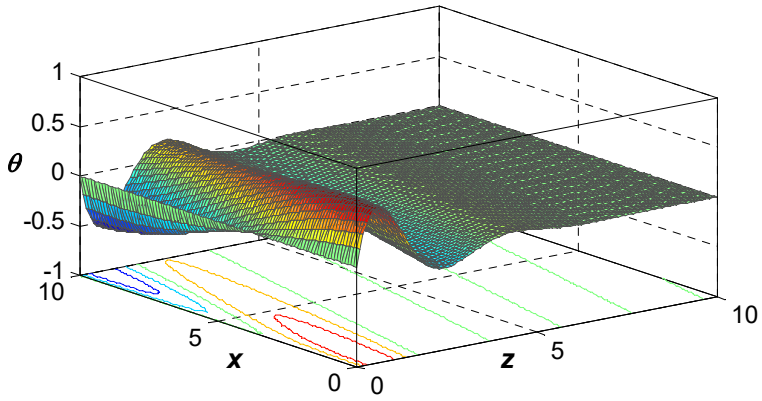



**Figure 15.** 3D distribution of thermodynamic temperature $\theta$ versus components of distance.

## 6. Conclusions

In the present study, we obtained from graphical results that the impact of the gravity field, reference temperature, and inclined load in a fiber-reinforced thermoelastic medium, via various forms of the modified Green–Naghdi framework play a great role in the thermoelasticity field. We obtained the following remarks:

(a) The consequences of reference temperature to all physical fields play a great role in increasing and decreasing the magnitude of these quantities.
(b) It is revealed that physical fields under consideration are sensitive to an inclined load.
(c) It is found that different physical fields under discussion are sensitive to the gravity field.
(d) The normal mode method with the eigenvalue approach that is used in the current study is applicable to a wide scope of problems in thermodynamics and thermoelasticity.
(e) It is revealed that physical fields under consideration are sensitive to the vertical distance.

**Author Contributions:** Conceptualization, S.M.S.; Methodology, S.M.S. and S.M.A.-D.; Software, S.M.S., E.K.J. and S.M.A.-D.; Validation, S.M.A.-D.; Formal analysis, S.M.S. and S.Y.A.; Investigation, S.M.S. and S.Y.A.; Resources, E.K.J., S.M.A.-D. and S.Y.A.; Data curation, E.K.J.; Writing—original draft, S.M.A.-D. and S.Y.A.; Writing—review & editing, S.M.S. and S.Y.A.; Visualization, S.M.S. and S.Y.A.; Supervision, E.K.J. and S.M.A.-D.; Project administration, E.K.J. All authors have read and agreed to the published version of the manuscript.

**Funding:** This work was supported and funded by the Deanship of Scientific Research at Imam Mohammad Ibn Saud Islamic University (IMSIU) (grant number IMSIU-DDRSP2602).

**Data Availability Statement:** The original contributions presented in this study are included in the article. Further inquiries can be directed to the corresponding author.

**Conflicts of Interest:** The authors declare no conflict of interest.

## Nomenclature

| | |
|---|---|
| $\sigma_{ij}$ | stress tensor |
| $e_{ij}$ | strain tensor |
| $T$ | thermodynamic temperature |
| $T_0$ | initial temperature $\left\|(\mathrm{T}-T_0)/T_0\right\|<1, \theta=T-T_0$. |
| $\lambda_0,\ \mu_0$ | constants of Lame |
| $\delta_{ij}$ | Kronecker's delta |
| $\alpha_t$ | thermal expansion constant, $\gamma=(3\lambda+2\mu)\,\alpha_t$ |
| $K$ | addition material constant |
| $K^*$ | thermal conductivity |
| $\alpha_0,\ \beta_0,\ (\mu_{L_0}-\mu_{T_0})$ | reinforcement variables |
| $\vec{b}=(b_1,\ b_2,\ b_3)$ | The fiber-direction is taken as $\vec{b}=(1,\ 0,\ 0). b_1^2+b_2^2+b_3^2=1$ |
| $\underline{u}$ | vector of displacement, $\underline{u}=(u_1,\ 0,\ u_3), \frac{\partial}{\partial y}=0$. |
| $\rho$ | density |
| $C_E$ | specific heat at rigid strain |
| i | $\mathrm{i}=\sqrt{-1}$ |
| $\varsigma$ | wave number |
| $m$ | complex magnitude |
| $\widetilde{u}(z)$ | physical amplitude of $u(z)$ |
| $\dot{\underline{u}}$ | particle velocity of the medium |
| $\tau_\theta$ | phase-lag for the temperature |
| $\tau_q$ | heat flux phase lag |
| $E$ | a non-dimensional key number |

## References


1. Biot, M. Thermoelasticity and irreversible thermodynamics. *J. Appl. Phys.* **1956**, *27*, 240–253. [CrossRef]
2. Belfield, A.J.; Rogers, T.G.; Spencer, A.J.M. Stress in elastic plates reinforced by fibres lying in concentric circles. *J. Mech. Phys. Solids* **1983**, *31*, 25–54. [CrossRef]
3. Chattopadhyay, A.; Choudhury, S. Magnetoelastic shear waves in an infinite self-reinforced plate. *Int. J. Num. Anal. Methods Geomech.* **1995**, *19*, 289–304.
4. Sengupta, P.R.; Nath, S. Surface waves in fibre-reinforced anisotropic elastic media. *Sadhana* **2001**, *26*, 363–370. [CrossRef]
5. Singh, B. Wave propagation in thermally conducting linear fibre-reinforced composite materials. *Arch. Appl. Mech.* **2006**, *75*, 513–520. [CrossRef]
6. Sarkar, N.; Atwa, S.Y. Two-temperature problem of a fiber-reinforced thermoelastic medium with a Mode-I crack under Green–Naghdi theory. *Microsyst. Technol.* **2018**, *24*, 1357–1367. [CrossRef]
7. Abbas, I.A. Generalized magneto–thermoelastic interaction in a fiber-reinforced anisotropic hollow cylinder. *Int. J. Thermophys.* **2012**, *33*, 567–579. [CrossRef]
8. Othman, M.I.A.; Said, S.M.; Marin, M. A novel model of plane waves of two-temperature fiber-reinforced thermoelastic medium under the effect of gravity with three-phase-lag model. *Int. J. Numer. Meth. Heat Fluid Flow* **2019**, *29*, 4788–4806. [CrossRef]
9. Alharbi, A.M.; Said, S.M.; Othman, M.I.A. The effect of multi-phase-lag and Coriolis acceleration on a fiber-reinforced isotropic thermoelastic medium. *Steel Comp. Struct.* **2021**, *39*, 125–134.
10. Kumar, R.; Sharma, S. A novel approach to fiber-reinforced composites with temperature-dependent properties using eigenvalue techniques. *Compos. Struct.* **2024**, *321*, 117–130.
11. Nandi, S.; Sarkar, S.P. A study on fiber-reinforced anisotropic materials with voids using the Moore–Gibson–Thompson thermoelastic model with memory effects. *Int. Commun. Heat Mass. Transf.* **2026**, *172*, 110524. [CrossRef]
12. Green, A.E.; Naghdi, P.M. Thermoelasticity without energy dissipation. *J. Elast.* **1993**, *31*, 189–208. [CrossRef]
13. Roychoudhuri, S.K.; Bandyopadhyay, N. thermoelastic wave propagation in a rotatingelastic medium without energy dissipation. *Int. J. Math. Math. Sci.* **2005**, *1*, 99–107.
14. Atwa, S.Y. Generalized magneto-thermoelasticity with two temperature and initial stress under Green–Naghdi theory. *Appl. Math. Model.* **2014**, *38*, 5217–5230. [CrossRef]
15. Abbas, I.A.; Alzahrani, F.S. A Green-Naghdi Model in a 2D Problem of a Mode I Crack in an Isotropic Thermoelastic Plate. *Phys. Mesomech.* **2018**, *21*, 99–103. [CrossRef]

16. Zenkour, A.M. Thermoelastic diffusion problem for a half-space due to a refined dual-phase-lag Green–Naghdi model. *J. Ocean Eng. Sci.* **2020**, *5*, 214–222. [CrossRef]
17. Othman, M.I.A.; Said, S.M. Gravity effects on thermoelastic materials under Green–Naghdi theory. *Steel Compos. Struct.* **2022**, *45*, 201–215.
18. Tzou, D.Y. A unified approach for heat conduction from macro-to micro-scales. *ASME J. Heat Transf.* **1995**, *117*, 8–16. [CrossRef]
19. Kutbi, M.A.; Zenkour, A.M. Refined dual-phase-lag Green–Naghdi models for thermoelastic diffusion in an infinite medium. *Waves Rand. Compl. Media* **2022**, *32*, 947–967. [CrossRef]
20. Zhou, J.; Zhang, X.; Zheng, Y.; Shen, X.; Li, Y. Research on longitudinal thermoelastic waves in an orthotropic anisotropic hollow cylinder based on the thermoelastic theory of Green–Naghdi. *Appl. Sci.* **2024**, *14*, 4952. [CrossRef]
21. Ailawalia, P.; Ajay; Marin, M.; Öchsner, A. A functionally graded Green-Naghdi (type-III) thermoelastic medium with varying properties along two directions. *Contin. Mech. Thermodyn.* **2025**, *37*, 58. [CrossRef]
22. Noda, N. Thermal stresses in materials with temperature-dependent properties. *Therm. Stress. I.* **1986**, *1*, 391–483.
23. Ezzat, M.A.; El-Karamany, A.S.; Samaan, A.A. The dependence of the modulus of elasticity on reference temperature in generalized thermoelasticity with thermal relaxation. *Appl. Math. Comput.* **2004**, *147*, 169–189. [CrossRef]
24. Othman, M.I.A.; Elmaklizi, Y.D.; Said, S.M. Generalized thermoelastic medium with temperature-dependent properties for different theories under the effect of gravity field. *Int. J. Thermophys.* **2013**, *34*, 521–553. [CrossRef]
25. Shakeriaski, F.; Ghodrat, M. Nonlinear response for a general form of thermoelasticity equation in mediums under the effect of temperature-dependent properties and short-pulse heating. *J. Therm. Anal. Calorim.* **2020**, *147*, 843–854. [CrossRef]
26. Luo, P.; Li, X.; Tian, X. Nonlocal thermoelasticity and its application in thermo-elastic problem with temperature-dependent thermal conductivity. *Eur. J. Mech. A/Sol.* **2021**, *87*, 104204. [CrossRef]
27. Deswal, S.; Sheoran, D.; Thakran, S.; Kalkal, K.K. Reflection of plane waves in a nonlocal microstretch thermoelastic medium with temperature dependent properties under three-phase-lag model. *Mech. Adv. Mater. Struct.* **2022**, *29*, 1692–1707. [CrossRef]
28. Abbas, I.A. Eigenvalue approach in a three-dimensional generalized thermoelastic interactions with temperature-dependent material properties. *Comp. Math. Appl.* **2014**, *68*, 2036–2056. [CrossRef]
29. Jain, K.; Kumar, S.; Deswala, S. Plane waves in nonlocal viscothermoelastic medium with temperature-dependent properties under three-phase-lag theory. *Waves Rand. Compl. Media* **2024**, *34*, 573–600. [CrossRef]
30. Said, S.M.; Jaradat, E.M.; Gafel, H.S.; Abo-Dahab, S.M. Outcome of Hall current and mechanical load on a fiber-reinforced thermoelastic medium per the hypothesis of one thermal relaxation time. *Crystals* **2025**, *15*, 924. [CrossRef]
31. Liu, J.; Hou, Z.; Liu, B.; Zhou, X. Mathematical and machine learning innovations for power systems: Predicting transformer oil temperature with Beluga whale optimization-based hybrid neural networks. *Mathematics* **2025**, *13*, 1785. [CrossRef]
32. Liu, J.; Duan, Z.; Hu1, X.; Zhong, J.; Yin, Y. Detracking autoencoding conditional generative adversarial network: Improved generative adversarial network method for tabular missing value imputation. *Entropy* **2024**, *26*, 402. [CrossRef] [PubMed]
33. Liu, J.; Hou, Z. Establishment of second-hand sailboats price prediction model based on random forest and exploration of influencing factors. In Proceedings of the 2023 IEEE 3rd International Conference on Data Science and Computer Application (ICDSCA), Dalian, China, 27–29 October 2023; pp. 1337–1342.
34. Das, N.C.; Lahiri, A. Eigenvalue approach to three dimensional coupled thermoelasticity in a rotating transversely isotropic medium. *Tamsui Oxf. J. Math. Sci.* **2009**, *25*, 237–257.
35. Lata, P.; Kaur, I. Effect of rotation and inclined load on transversely isotropic magneto thermoelastic solid. *Struct. Eng. Mech.* **2019**, *70*, 245–255.

**Disclaimer/Publisher's Note:** The statements, opinions and data contained in all publications are solely those of the individual author(s) and contributor(s) and not of MDPI and/or the editor(s). MDPI and/or the editor(s) disclaim responsibility for any injury to people or property resulting from any ideas, methods, instructions or products referred to in the content.